Advanced Robotics

ISSN: 0169-1864 (Print) 1568-5535 (Online) Journal homepage: http://www.tandfonline.com/loi/tadr20

Optimization design of general triglide parallel manipulators

S. J. Yan, S. K. Ong & A. Y. C. Nee

To cite this article: S. J. Yan, S. K. Ong & A. Y. C. Nee (2016) Optimization design of general triglide parallel manipulators, Advanced Robotics, 30:16, 1027-1038, DOI: 10.1080/01691864.2016.1192063

To link to this article: http://dx.doi.org/10.1080/01691864.2016.1192063

Published online: 10 Jun 2016.

Submit your article to this journal

Article views: 162

View related articles

View Crossmark data

Full Terms & Conditions of access and use can be found at
http://www.tandfonline.com/action/journalInformation?journalCode=tadr20

Download by: [Tel Aviv University] **Date:** 05 November 2017, At: 02:41

ADVANCED ROBOTICS, 2016
VOL. 30, NO. 16, 1027–1038
http://dx.doi.org/10.1080/01691864.2016.1192063

RSJ Taylor & Francis
Taylor & Francis Group

FULL PAPER

Optimization design of general triglide parallel manipulators

S. J. Yan, S. K. Ong and A. Y. C. Nee

Mechanical Engineering Department, National University of Singapore, Singapore, Singapore

ABSTRACT

Optimization design of parallel manipulators has attracted much interest from researchers in recent years. The reported methodologies attempted to achieve optimal design of parallel manipulators considering several properties, such as dexterity, stiffness, and space utilization, which are important parameters to be considered. However, stiffness analysis considered by many researchers generally ignores the deformation of the mobile platform. For space utilization, there is no reported method to consider the variation in the physical size caused by different postures of the manipulator. Additionally, although optimization of a linear delta and an orthoglide has been presented by several researchers, optimization of a general triglide has not been reported. In order to address these issues, this paper presents a multi-objective optimization addressing dexterity, stiffness, and space utilization of a general triglide. Its stiffness matrix is obtained considering the deformation of mobile platform, limbs, and actuators. A novel stiffness index is used to evaluate its stiffness property considering external wrench applied on the manipulator. The physical size of the triglide is represented using both a constant size and a variable size. Comparing with a reported optimization methodology, it is proven that the proposed method is capable of providing optimal solutions with better properties.

ARTICLE HISTORY
Received 8 April 2015
Revised 16 January 2016
Accepted 27 April 2016

KEYWORDS
Multi-objective optimization; triglide parallel manipulator; dexterity; stiffness analysis; space utilization; variable dimension

Downloaded by [Tel Aviv University] at 02:41 05 November 2017

1. Introduction

As parallel manipulators present good performance in terms of accuracy, rigidity, and load-weight ratio, they can be applied in precision machining, medical surgery, pick-and-place operation, and other fields.[1] The performance analysis of a parallel manipulator is complex; however, a good optimization design approach is able to bring significant improvements. Since it imposes high computation load for an optimization strategy considering exhaustive properties of a parallel manipulator, many researchers optimize one or a few properties. These properties are generally represented and evaluated using specific indices.

Prior to the design of a parallel manipulator, its dexterity is considered to be an important performance property. This property assesses positioning accuracy, singularity, and local isotropy. Several indices have been used to represent the dexterity property, such as the manipulability,[2–4] the determinant [5], and the condition number of the Jacobian matrix.[6–9] Since the Jacobian matrix depends on the configuration of a manipulator, the condition number presents only a local property, while Gosselin and Angeles [10] proposed a novel index to give a global property measurement. This index has been widely used to measure the dexterity for the optimization of parallel manipulators.[11–16] Due to its wide application and easy implementation, this index is also adopted in this paper to study the dexterity property.

Although parallel manipulators present good performance in terms of accuracy and rigidity, it is still necessary to consider the stiffness in the optimization design, as the stiffness of a parallel manipulator is greatly dependent on its structural configuration. This property has been optimized by many researchers. However, most of these researchers only considered the compliance of the actuators. For example, Liu [12], Kelaiaia et al. [17], Chi and Zhang [18], and Gao et al. [19] took into account only the actuator stiffness to obtain the stiffness matrix of a parallel manipulator. El-Khasawneh and Ferreira [20] integrated the compliance of the limb and the compliance of the actuator into the stiffness analysis of a Stewart platform. Klimchik et al. [21] used a virtual joint modeling method to analyze the stiffness of serial chains and applied this method into the stiffness analysis of parallel manipulators [22] under external and internal loads. This method was also adopted by Kucuk [23] for the stiffness analysis of a planar parallel manipulator. In this analysis, the stiffness

CONTACT S. K. Ong mpeongsk@nus.edu.sg

© 2016 Taylor & Francis and The Robotics Society of Japan

Downloaded by [Tel Aviv University] at 02:41 05 November 2017

of the mobile platform is computed using the model of a cantilever beam. Cheng et al. [24] found that the deformation of a parallel manipulator obtained using a finite element method for stiffness analysis is larger than that obtained using an algebraic method, in which the actuator and the limb are assumed to be flexible. Based on this finding, Cheng et al. [24] mentioned that the difference is due to neglecting the deformation of the mobile platform. Therefore, it is more accurate to integrate the deformation of the mobile platform, the limbs, and actuators in stiffness optimization.

Another important property of a parallel manipulator is its space utilization. This property reflects the physical size of a manipulator's structure. Several researchers [3,12,15] used a ratio of the workspace volume to the physical size to measure this property. A higher value of the ratio represents the capability of a parallel manipulator to achieve larger workspace with more compact structure. To obtain the ratio, the physical size is generally approximated using a regular shape. For example, Stock and Miller [3] used a bounding box and Rao et al. [15] used a least cylinder enclosing a parallel manipulator and its workspace. This approximation increases the physical size and it cannot reflect the real physical size which is changing due to the different postures of the manipulator.

Additionally, the optimization of a linear delta and an orthoglide has been presented [25–27]; however, the optimization of a general triglide has not been reported. The linear delta and the orthoglide have similar structures. The difference between them is the tilting angles of the actuators against their base plates. In this paper, the parallel manipulators having similar structures with the orthoglide but different tilting angles are grouped as triglide parallel manipulators.

With these gaps described in this section, this paper presents an optimization methodology to improve general triglides for their dexterity, stiffness, and space utilization. The stiffness analysis considers the deformation of the mobile platform, limbs, and actuators. In order to obtain accurately the physical size of a general triglide, its size is separated into a constant size and a variable size. The variable size is obtained using the average of spatial dimensions of the triglide in different postures. In addition, a novel stiffness index is used to measure the stiffness property. This index relates its value to the direction of the wrench experienced by the mobile platform of a triglide in an operation. With this index, the resistance of a triglide to deformation under a given wrench can be measured easily.

It should be noted that the optimization proposed in this paper incorporates three different objective functions. The multi-objective optimization can be solved by aggregating all the objectives into a scalar function using weighting parameters. Although this method can produce a single solution without interaction with the users, the solution is highly dependent on the setting of the weighting parameters which are unknown prior to optimization. [28] In practice, the user may need to perform the optimization many times using different settings of weighting parameters to obtain different solutions until an appropriate solution is found. Compared with this method, a Pareto method attempts to find a set of trade-off solutions in the objective space. Once the trade-off hyper-surface of the solutions is obtained, the user can select an appropriate design considering other requirements. To obtain the hyper-surface, a non-dominance sorting genetic algorithm (NSGA) proposed in [29] has claimed to have better performance in achieving both convergence and diversity of solutions. Therefore, the NSGA algorithm is used in this paper to achieve the trade-off solutions.

This paper is organized as follows. A description of the structure of a general triglide is presented in Section 2. Section 3 describes the indices of dexterity, stiffness, and space utilization, followed by the proposed objectives, variables, constraints, and solution algorithm which are illustrated in Section 4. Section 5 uses the proposed methodology to provide optimal design for a general triglide with a comparison to a reported optimal solution of a parallel manipulator, which has a similar structure as the triglide. Section 6 compares the stiffness of one optimal solution obtained using the proposed methodology to that of the reported solution using a finite element analysis (FEA) method. Finally, Section 7 summarizes the results and contributions presented in this paper.

2. Triglide manipulator

In the class of 3-DOF pure translational parallel manipulators, the delta robot may be the most known manipulator. It was first patented in 1990s [30] and has been applied for picking and packaging operations. The orientation of the mobile platform of the delta robot is well constrained by a parallelogram structure. After the delta robot, the parallelogram structure was adopted by several researchers to construct the limbs of a linear delta [31] and an orthoglide,[32] by replacing the rotary actuators with translational actuators. If α denotes the angle between the actuator axis and the base plate, $\alpha = \pi/2$ radians for the linear delta, and $\alpha = 0.6155$ radian for the orthoglide. A general triglide is defined to be a parallel manipulator which has a similar structure with the orthoglide, but the angle α is arbitrary. The structure of a general triglide is depicted in Figure 1. With this definition, the linear delta and the orthoglide are two particular triglides. Except $\alpha = \pi/2$ radians, the actuator axes of a general triglide intersect at one point in space.

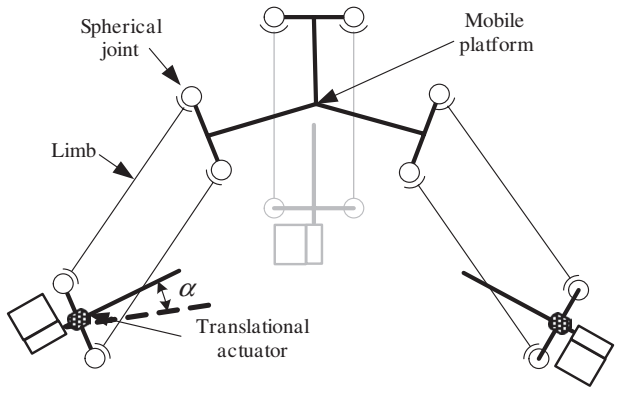

Figure 1. The structure of a general triglide.

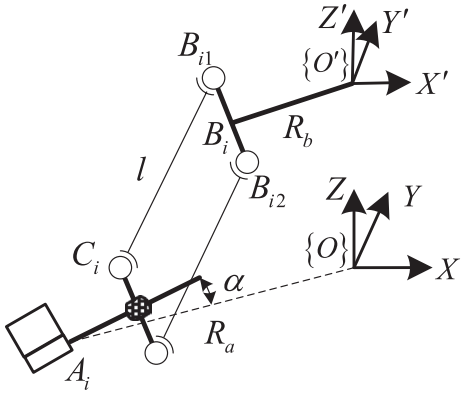

Figure 2. The structure of one limb of a triglide.

3. Performance indices

The dexterity, stiffness, and space utilization are considered in this paper to improve the performance of a general triglide, since they are important properties and widely adopted by many researchers.

3.1. Dexterity

Singularity avoidance is one important requirement of a parallel manipulator during a task. In order to assess singularity avoidance and position accuracy, the dexterity property is measured using the condition number of the kinematic Jacobian matrix. Before the calculation of the dexterity index, it is necessary to obtain the Jacobian matrix first. Figure 2 depicts the structure of one limb of a general triglide. If t_i denotes the unit vector of B_iC_i, $\dot{x}$ and $\dot{q}_i$ denote, respectively, the velocity of the mobile platform and the ith actuator, and s_i is the unit vector of A_iC_i, Equation (1) can be obtained.

$$t_i^T \dot{x} = t_i^T s_i \dot{q}_i \tag{1}$$

The forward kinematic Jacobian matrix is obtained using Equation (2), and the inverse kinematic Jacobian matrix is obtained using Equation (3).

$$\mathbf{J}_q = \begin{bmatrix} t_1^T s_1 & & \\ & t_2^T s_2 & \\ & & t_3^T s_3 \end{bmatrix} \tag{2}$$

$$\mathbf{J}_x = \begin{bmatrix} t_1 & t_2 & t_3 \end{bmatrix}^T \tag{3}$$

Therefore, the Jacobian matrix can be obtained using Equation (4).

$$\mathbf{J} = \mathbf{J}_x^{-1}\mathbf{J}_q \tag{4}$$

Since the Jacobian matrix is dependent on the postures of the triglide, the condition number reflects the local dexterity property. In order to measure the global property, the global dexterity index (GDI) can be calculated using Equation (5), where k is the condition number, which can be obtained using $k = \|\mathbf{J}^{-1}\|\|\mathbf{J}\|$, and Φ is the entire workspace of the triglide.

$$\eta = \frac{\int_W \frac{1}{\kappa} d\Phi}{\int_W d\Phi} \tag{5}$$

Since k tends to infinity at singularities, and is equal to 1 at isotropic positions, the global GDI is within the interval $[0, 1]$ and larger value of η gives better dexterity of the triglide.

3.2. Stiffness

Stiffness is crucially related to the accuracy and payload of a parallel manipulator, since stiffness reflects the direct mapping between the externally applied wrench and the deformation of the manipulator. This paper uses a strain energy method considering the compliances of the mobile platform, the limbs, and the actuators of a triglide to obtain the stiffness matrix.

Equation (6) shows the relationship of the external wrench $\mathbf{W}$ and the corresponding infinitesimal twist $\delta\boldsymbol{\xi}$ of the central point of the mobile platform of the triglide, where $\mathbf{K}$ denotes the stiffness matrix of the triglide.

$$\mathbf{W} = \mathbf{K}\delta\boldsymbol{\xi} \tag{6}$$

If only elastic deformation is considered, according to Castigliano's second theorem, Equation (7) can be obtained, where U denotes the strain energy stored in the structure of a triglide.

Downloaded by [Tel Aviv University] at 02:41 05 November 2017

Downloaded by [Tel Aviv University] at 02:41 05 November 2017

$$\delta\boldsymbol{\xi} = \frac{\partial U}{\partial \mathbf{W}} \tag{7}$$

With the external wrench $\mathbf{W}$ as shown in Figure 3, the reaction forces $\mathbf{f}$ exerted to the mobile platform can be obtained using Equation (8), where $\mathbf{f} = \begin{bmatrix} f_{11} & f_{12} & f_{21} & f_{22} & f_{31} & f_{32} \end{bmatrix}^T$ and $\mathbf{A}$ is the inverse compliant Jacobian matrix.

$$\mathbf{f} = \mathbf{A}\mathbf{W} \tag{8}$$

To obtain the strain energy U, this paper assumes that the mobile platform, the parallelogram-type limbs and the actuators are flexible, while the other components are infinitely rigid. With the reaction forces on the mobile platform, an arbitrary cross section of the mobile platform experiences an axial force f_{ix}, two shear forces f_{iy}, f_{iz}, and three moments M_{ix}, M_{iz}, τ_i, as depicted in Figure 4. The forces and moments can be obtained using Equation (9). In this equation, f_{ij} denotes one reaction force in the vector $\mathbf{f}$, $\mathbf{l}_i$ denotes the unit vector of the ith limb, $\mathbf{q}_i$ denotes the unit vector of $O'O_i$, $\mathbf{b}_{i1}$ denotes the unit vector of O_iB_{i1}, b_{i1}, and b_{i2} denote the lengths of vectors O_iB_{i1} and O_iB_{i2}, and v_i denotes the distance of the cross section to the connection point between the mobile platform and the limb.

$$\begin{cases} f_{ix} = (f_{i1} + f_{i2})\boldsymbol{l}_i \cdot \boldsymbol{b}_{i1} \\ f_{iy} = (f_{i1} + f_{i2})\boldsymbol{l}_i \cdot \boldsymbol{q}_i \\ f_{iz} = (f_{i1} + f_{i2})\boldsymbol{l}_i \cdot (\boldsymbol{b}_{i1} \times \boldsymbol{q}_i) \\ M_{ix} = v_i(f_{i1} + f_{i2})\boldsymbol{l}_i \cdot (\boldsymbol{b}_{i1} \times \boldsymbol{q}_i) \\ M_{iz} = (b_{i2}f_{i2} - b_{i1}f_{i1})\boldsymbol{l}_i \cdot \boldsymbol{q}_i + v_i(f_{i1} + f_{i2})\boldsymbol{l}_i \cdot \boldsymbol{b}_{i1} \\ \tau_i = (b_{i1}f_{i1} - b_{i2}f_{i2})\boldsymbol{l}_i \cdot (\boldsymbol{b}_{i1} \times \boldsymbol{q}_i) \end{cases} \tag{9}$$

With the internal forces and moments, the strain energy of the mobile platform can be obtained using Equation (10).

$$U_{MP} = \sum_{i=1}^{3} \int_0^{R_{bi}} \left[\frac{M_{ix}^2}{2E_{MP}I_{xx,MP}} + \frac{M_{iz}^2}{2E_{MP}I_{zz,MP}} + \frac{\tau_i^2}{2G_{MP}J_{MP}} + \frac{f_{iy}^2}{2E_{MP}A_{MP}} + \frac{f_{ix}^2}{2G_{MP}A_{x,MP}} + \frac{f_{iz}^2}{2G_{MP}A_{z,MP}} \right] \mathrm{d}v_i \tag{10}$$

In Equation (10), E_{MP} and G_{MP} denote the elastic modulus and the shear modulus of the mobile platform; $I_{xx,MP}$ and $I_{zz,MP}$ denote the area moment of inertia of the cross section about the x and z axes; J_{MP} denotes the polar moment of inertia of the cross section; A_{MP} denotes the area of the cross section; $A_{x,MP}$ and $A_{z,MP}$ denote the effective shear area of the cross section along the x and z axes.

For simplicity, Equation (11) can be obtained using Equations (9) and (10).

$$U_{MP} = \sum_{i=1}^{3} \mu_{MP1,i}f_{i1}^2 + \mu_{MP2,i}f_{i1}f_{i2} + \mu_{MP3,i}f_{i2}^2 \tag{11}$$

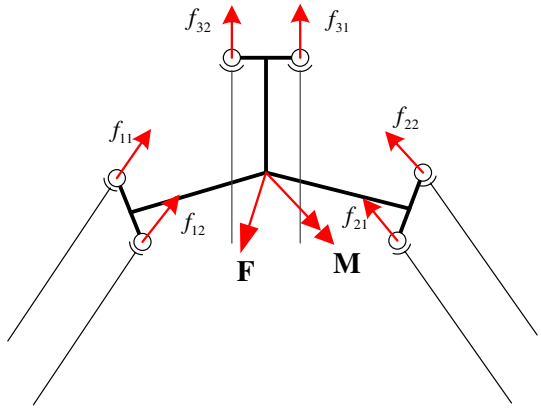

Figure 3. The applied external wrench and reaction forces on the mobile platform.

Similar to the mobile platform, the strain energy U_{PL} stored in the limbs and U_{Act} in the actuators can be obtained using Equations (12) and (13).

$$U_{PL} = \sum_{i=1}^{3} \left(\mu_{PL1,i}f_{i1}^2 + \mu_{PL2,i}f_{i1}f_{i2} + \mu_{PL3,i}f_{i2}^2 \right) \tag{12}$$

$$U_{Act} = \sum_{i=1}^{3} \left(\mu_{Act1,i}f_{i1}^2 + \mu_{Act2,i}f_{i1}f_{i2} + \mu_{Act3,i}f_{i2}^2 \right) \tag{13}$$

In Equations (11) to (13), $\mu_{MP1,i}$, $\mu_{MP2,i}$, $\mu_{MP3,i}$, $\mu_{PL1,i}$, $\mu_{PL2,i}$, $\mu_{PL3,i}$, and $\mu_{Act1,i}$, $\mu_{Act2,i}$, $\mu_{Act3,i}$ are stiffness coefficients specifically dependent on the geometrical and physical properties of the mobile platform, the limbs and the actuators. Please refer to [33] for more details about the computation of these coefficients.

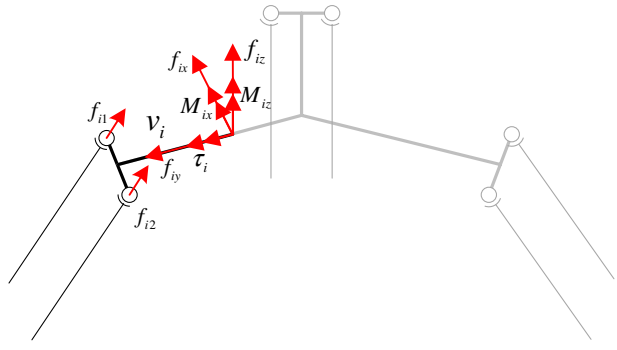

Figure 4. Internal forces and moments experienced by a cross section of the mobile platform.

Downloaded by [Tel Aviv University] at 02:41 05 November 2017

Hence, if $\mu_{1,i} = \mu_{MP1,i} + \mu_{PL1,i} + \mu_{Act1,i}$, $\mu_{2,i} = \mu_{MP2,i} + \mu_{PL2,i} + \mu_{Act2,i}$ and $\mu_{3,i} = \mu_{MP3,i} + \mu_{PL2,i} + \mu_{Act3,i}$, the total strain energy U is obtained using Equation (14).

$$U = \sum_{i=1}^{3} \left(\mu_{1,i} f_{i1}^2 + \mu_{2,i} f_{i1} f_{i2} + \mu_{3,i} f_{i2}^2 \right) \tag{14}$$

If $a_{i,j}$ denotes the element located in the ith row and jth column of the inverse compliant Jacobian matrix $\mathbf{A}$, and $\mathbf{a}_i$ denotes the ith row vector of the matrix $\mathbf{A}$, the partial derivative of the strain energy with respect to the external wrench can be obtained using Equation (15).

$$\frac{\partial U}{\partial \mathbf{W}} = \mathbf{C}\mathbf{W} \tag{15}$$

$\mathbf{C}$ is the overall compliance matrix given as follows.

$$\mathbf{C} = \begin{bmatrix} \sum_{i=1}^{3} (2\mu_{1,i} a_{2i-1,1} \mathbf{a}_{2i-1} + \mu_{2,i} a_{2i-1,1} \mathbf{a}_{2i} + \mu_{2,i} a_{2i,1} \mathbf{a}_{2i-1} + 2\mu_{3,i} a_{2i,1} \mathbf{a}_{2i}) \\ \sum_{i=1}^{3} (2\mu_{1,i} a_{2i-1,2} \mathbf{a}_{2i-1} + \mu_{2,i} a_{2i-1,2} \mathbf{a}_{2i} + \mu_{2,i} a_{2i,2} \mathbf{a}_{2i-1} + 2\mu_{3,i} a_{2i,2} \mathbf{a}_{2i}) \\ \sum_{i=1}^{3} (2\mu_{1,i} a_{2i-1,3} \mathbf{a}_{2i-1} + \mu_{2,i} a_{2i-1,3} \mathbf{a}_{2i} + \mu_{2,i} a_{2i,3} \mathbf{a}_{2i-1} + 2\mu_{3,i} a_{2i,3} \mathbf{a}_{2i}) \\ \sum_{i=1}^{3} (2\mu_{1,i} a_{2i-1,4} \mathbf{a}_{2i-1} + \mu_{2,i} a_{2i-1,4} \mathbf{a}_{2i} + \mu_{2,i} a_{2i,4} \mathbf{a}_{2i-1} + 2\mu_{3,i} a_{2i,4} \mathbf{a}_{2i}) \\ \sum_{i=1}^{3} (2\mu_{1,i} a_{2i-1,5} \mathbf{a}_{2i-1} + \mu_{2,i} a_{2i-1,5} \mathbf{a}_{2i} + \mu_{2,i} a_{2i,5} \mathbf{a}_{2i-1} + 2\mu_{3,i} a_{2i,5} \mathbf{a}_{2i}) \\ \sum_{i=1}^{3} (2\mu_{1,i} a_{2i-1,6} \mathbf{a}_{2i-1} + \mu_{2,i} a_{2i-1,6} \mathbf{a}_{2i} + \mu_{2,i} a_{2i,6} \mathbf{a}_{2i-1} + 2\mu_{3,i} a_{2i,6} \mathbf{a}_{2i}) \end{bmatrix}$$

After obtaining the total compliant matrix $\mathbf{C}$, the total stiffness matrix $\mathbf{K}$ can be obtained.

$$\mathbf{K} = \mathbf{C}^{-1} \tag{16}$$

In the optimization stage, the stiffness matrix is required to be converted to a stiffness index to evaluate the stiffness property of a parallel manipulator. Generally, the maximum and minimum eigenvalues,[34–36] the determinant,[35] the Euclidean norm of the diagonal elements [37], and the condition number [38] of the stiffness matrix can be accepted as stiffness indices. These indices cannot be interpreted easily, since the translation and orientation of a parallel manipulator have different units. Additionally, these stiffness indices fail to relate the stiffness property of a parallel manipulator to the direction of a wrench applied on it. This paper uses a novel stiffness index, which measures the inverse of the virtual work completed by a unit wrench, to evaluate the stiffness of a triglide. Supposing the unit wrench is $\mathbf{W}_u$ and $\mathbf{K}^{-1}$ is the inverse of the stiffness matrix, the stiffness index is defined using Equation (17). For the same $\mathbf{W}_u$, the stiffer manipulator has smaller deformations, which causes smaller virtual work, so that the index obtained using Equation (17) is larger, since the stiffness matrix is positive semidefinite.

$$\kappa_V = \frac{1}{\mathbf{W}_u^T \mathbf{K}^{-1} \mathbf{W}_u} \tag{17}$$

Since the stiffness matrix is dependent on the postures of a triglide, the stiffness index is a local presentation of the stiffness property. In order to measure the global stiffness property, the global stiffness index (GSI) is obtained using Equation (18).

$$\eta_\kappa = \frac{\int_W \kappa_V \mathrm{d}\Phi}{\int_W \mathrm{d}\Phi} \tag{18}$$

3.3. Space utilization

The space utilization of a triglide is measured using the ratio of its workspace volume to its physical size (RWV). The workspace volume can be obtained using inverse kinematics and represented by point cloud which can be reached by the mobile platform of the triglide. The physical size can be separated into a constant size and a variable size as shown in Figure 4. Since the triglide is a three-limb parallel mechanism, triangular prisms are used to represent its physical size. The volume of the constant prism remains the same, while the volume of the variable prism depends on the postures of the triglide. If the constant volume is denoted by V_1, it can be obtained using Equation (19), in which R_a denotes the radius of the base plate and s_d is the full stroke of the actuator.

$$V_1 = \frac{\sqrt{3}}{4} \left(3R_a^2 s_d \sin\alpha + 3R_a s_d^2 \sin\alpha \cos\alpha + s_d^3 \sin\alpha \cos^2\alpha \right) \tag{19}$$

The variable prism is not a real prism since any two instances of B_1C_1, B_2C_2, and B_3C_3 are not absolutely coplanar. If V_2 denotes the variable volume, it can be computed

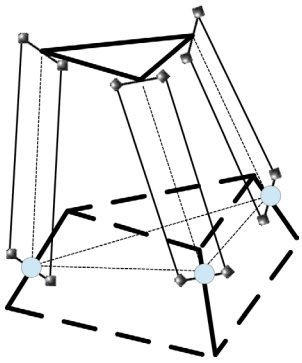

a) Structure of the triglide

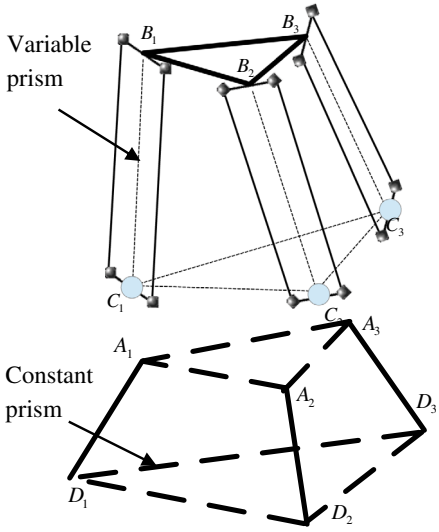

b) The constant prism and the variable prism

Figure 5. The triglide's structure and its constant prism and variable prism (a) Structure of the triglide (b) The constant prism and the variable prism.

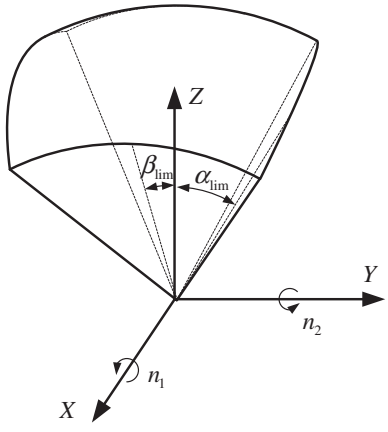

Figure 6. The motion range of rotations of a parallelogram limb.

as the sum of the volumes of three triangular pyramids $B_1 - C_1C_2C_3$, $C_2 - B_1B_2B_3$, and $B_1 - B_3C_2C_3$. Since V_2 is changing due to the movement of the mobile platform, its average value over the workspace is used. As shown in Figure 5(a), the volumes V_1 and V_2 have an overlapped volume, which is the volume of prism $A_1A_2A_3 - C_1C_2C_3$. If the overlapped volume is denoted by V_3, the RWV can be obtained using Equation (20). Larger ratio reflects better space utilization of the manipulator, where V denotes the workspace volume.

$$\eta_V = \frac{2V}{V_1 + \frac{\int_W V_2 - V_3 \mathrm{d}\Phi}{\int_W \mathrm{d}\Phi}} \tag{20}$$

4. Architecture optimization

4.1. Design variables

An exhaustive description of a general triglide needs tens of variables. The optimization of all these variables is complicated and time-consuming. Since a practical triglide is symmetrical in general, five variables can be used to construct a symmetrical triglide, including the radius R_a of the base plate, the radius R_b of the mobile platform, the limb length l, the tilting angle α, and the full stroke s_d of the actuator. Hence, the design variables are $\mathbf{X} = [\ R_a \quad R_b \quad l \quad \alpha \quad s_d\ ]^T$.

4.2. Constraints

In the design of a general triglide, some physical constraints should be taken into consideration, such as the motion range of passive joints. If the parallelogram limb is considered as one integrated part, each limb has two rotation DOFs, so that the physical constraint posed by the passive joints allows rotation angles about two axes smaller than $\alpha_{\lim}$ and $\beta_{\lim}$ as shown in Figure 6.

Besides the constraint due to the motion range of the passive joints, collision among all the limbs of the triglide should be avoided in the movement of the mobile platform. If all the limbs are simplified as identical solid cylinders, collision-free movement can be achieved by ensuring that the shortest distance between any two limbs is larger than the diameter of the limb.

It is common to define a prescribed task space before the optimization of a parallel manipulator to guarantee that the manipulator can complete an expected task in practice. To satisfy this constraint, the prescribed task space is discretized into a point cloud and every point will be verified to check whether it can be reached by the mobile platform.

4.3. Objective function

Since this research aims to optimize the dexterity, stiffness, and space utilization of a general triglide, the

Downloaded by [Tel Aviv University] at 02:41 05 November 2017

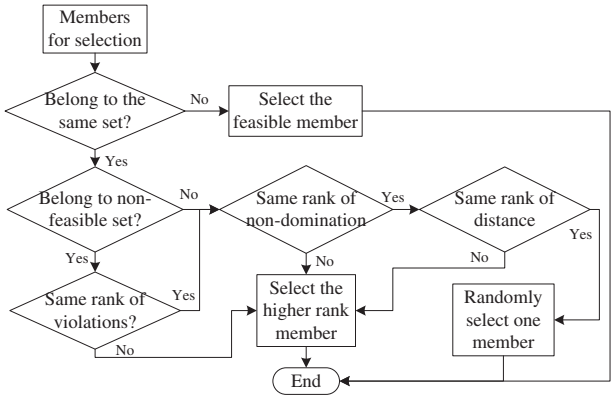

Figure 7. The selection principle of the NSGA.

optimization can be formulated into Equation (21), where $\mathbf{F} = \begin{bmatrix} \eta & \eta_\kappa & \eta_V \end{bmatrix}^T$ and $\mathbf{C}_t$ denotes the constraints posed by the motion range of passive joints and the requirements of collision avoidance and specified task space.

$$\begin{cases} \max \mathbf{F}(\mathbf{X}) \\ \mathbf{C}_t \leq 0 \end{cases} \tag{21}$$

4.4. Solution algorithm

The NSGA algorithm is used to solve the multi-objective optimization. The populations in each generation are grouped into feasible and non-feasible sets based on the constraints. The members in the feasible set are first sorted according to the level of non-domination, and later sorted using the distance of the objective values of each member to its neighbors in the space of objective functions. A member with a higher rank of non-domination means there are fewer other members that are better than it, and a higher rank of the distance provides better diversity of the populations. The non-feasible set is first sorted based on the violation numbers of the constraints. A member with fewer violations is assigned a higher rank. The following sorting procedure is the same as the feasible set. More information about the NSGA algorithm can be found in [29]. During the genetic operation, the selection follows the principles depicted in Figure 7.

5. Optimization comparison

In order to evaluate the proposed optimization method for a general triglide, it is compared to a method proposed in [39], in which a purely translational parallel manipulator was optimized to improve its dexterity and space utilization. The authors aggregated the objectives into a scalar function using weight parameters to solve the optimization. One optimal solution, which was obtained using equal weight parameters of the dexterity and space utilization, is selected for the comparison. This solution is labeled as Ref. 1. The variable values of Ref. 1 are listed in Table 1. Since the stiffness was not considered in [39], the GSI of Ref. 1 is obtained using the method introduced in Section 3. As discussed in Section 3, the stiffness analysis requires the geometrical and physical properties of the manipulator. For simplicity, the mobile platform, the limbs, and the leads of the actuators are constructed using identical spherical solid beams. Their properties are listed in Table 2. Since the calculation of the GSI requires a unit

Table 1. Variable values of Refs. 1 and 2.

	R_a/(mm)	R_b/(mm)	l/(mm)	α/(°)	s_d/(mm)
Ref. 1	3	1	3	45	2
Ref. 2	2.96	1.02	3.76	88.68	2

Table 2. The geometrical and physical properties of the optimized parallel manipulator.

A_b/mm^2 (Cross section area of the solid beams)	3.1416
E/GPa (Elastic modulus of the solid beams)	210
G/GPa (Shear modulus of the solid beams)	80
N (Transmission ratio of the gear box used in actuators)	5
P/mm (Lead of the lead screw used in actuators)	3
k_{tor}/N · m/rad (Equivalent stiffness of the motor)	3×10^5

Table 3. Design variables and constraints.

Design variables	R_a/mm	$1 \leq R_a \leq 8$
	R_b/mm	$1 \leq R_b \leq 8$
	l/mm	$2 \leq l \leq 8$
	α/degree	$0 \leq \alpha \leq 105$
Constant variable	s_d/mm	2
Motion range	α_{lim}/degree	40
	β_{lim}/degree	40
Other constraints		$R_a > R_b$

Downloaded by [Tel Aviv University] at 02:41 05 November 2017

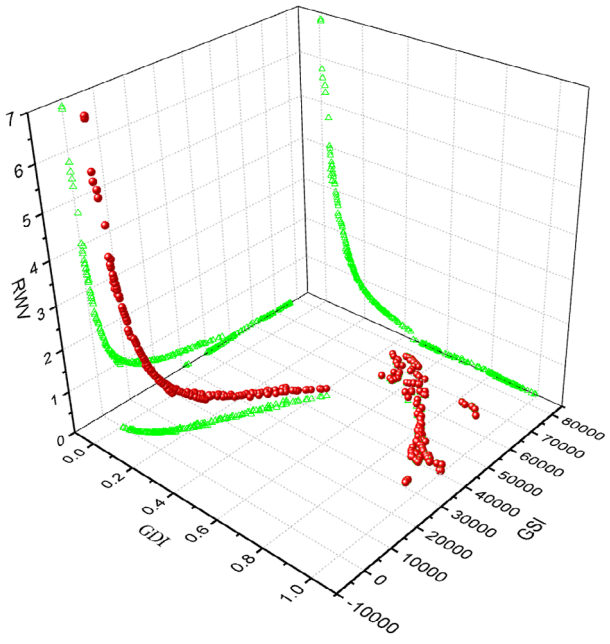

Figure 8. The Pareto front obtained using the NSGA algorithm.

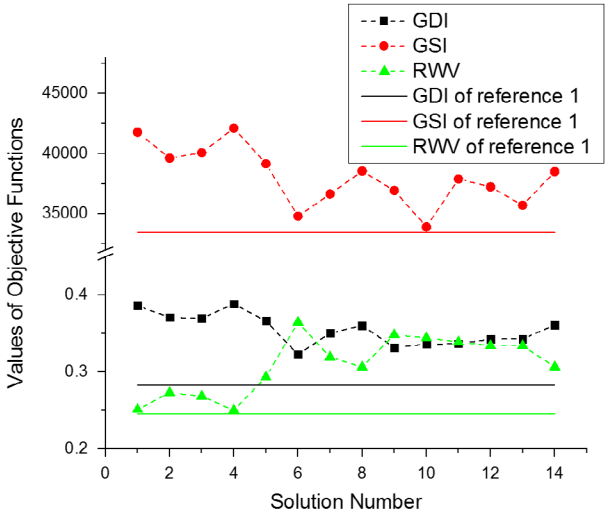

Figure 9. The objective values of Refs. 1 and 14 optimal solutions.

wrench, the applied wrench on the mobile platform is defined to be $\begin{bmatrix} 0 & 0 & \sqrt{2}/2 & 0 & 0 & \sqrt{2}/2 \end{bmatrix}$, which means the mobile platform experiences a force in the z direction and a torque against the z axis. To make the comparison convincing, the optimization in this paper adopts the same constraints and the same design variables as used in [39] and they are listed in Table 3. The optimization includes four variables, which are the radii R_a and R_b of the base plate and the mobile platform, limb length l and tilting angle α. The stroke of the actuator is defined to be a constant and its value is set as 2.

In addition, the number of populations in each generation is set as 200, and the total generations are 1000 in the NSGA algorithm. This optimization algorithm is implemented using MatLab (Mathworks, Inc).

Figure 8 depicts the Pareto front obtained in the 1000th generation and its projection on three coordinate planes. From Figure 8, it can be seen that the RWV is conflicting with the GDI and GSI. It is impossible to achieve optimal RWV, GDI, and GSI simultaneously. It is also found that the GDI and GSI are nearly harmonious when the GDI is less than about 0.5, but they become conflicting as the GDI becomes larger. Due to the complex relationship among these three properties, the NSGA algorithm is capable of providing various solutions. With these solutions, the user can select the appropriate one based on other requirements. If the requirement is set to be better than Refs. 1, 14 solutions are found from the Pareto front. The values of objective functions of these solutions are depicted in Figure 9. It can be seen that the objective values of all the solutions are better than those reported in Ref. 1.

It should be noted that the optimization compared to Ref. 1 does not include the stroke s_d. However, the stroke is believed to have significant effect on the performance of a parallel manipulator. Thus, the stroke is contained into the design variables and the optimization is performed again. The boundary of the stroke is defined to be $2 \le s_d \le 8$. In this optimization, 1 of the 14 optimal solutions plotted in Figure 9 is selected as in Ref. 2. Its variable values are listed in Table 1. This solution has the largest values of the GDI and GSI in all the 14 solutions. Compared to Ref. 2, seven optimal solutions are obtained from the new optimization. Their objective values are depicted in Figure 10, which shows that these optimal solutions are better than Ref. 2. With Figures 9 and 10, it is shown that the optimization proposed in this paper can provide better solutions as compared to the method proposed in [39], and the inclusion of the stroke into the design variables is able to improve the optimal solutions further.

6. Stiffness comparison using a FEA method

As shown in Figure 9, the stiffness of Ref. 2 is better than that of Ref. 1. In order to evaluate Refs. 1 and 2, FEA

Table 4. The configurations of Refs. 1 and 2 analyzed using the FEA method.

Manipulator	Actuator	Units	Symmetric configuration	Asymmetric configuration
Refs. 1 and 2	Actuator 1	mm	3	1
	Actuator 2	mm	3	2
	Actuator 3	mm	3	3

Downloaded by [Tel Aviv University] at 02:41 05 November 2017

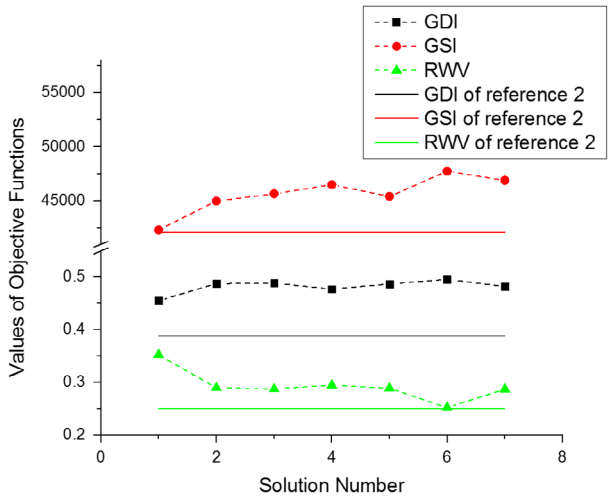

Figure 10. The objective values of Ref. 2 and the seven optimal solutions.

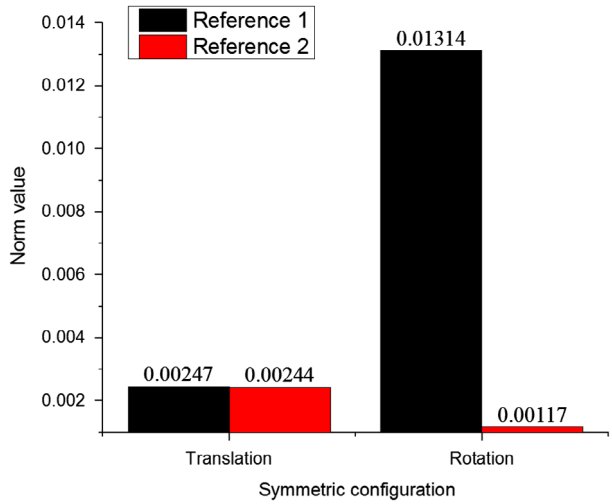

Figure 11. Deformation comparison of Refs. 1 and 2 in the symmetric configuration.

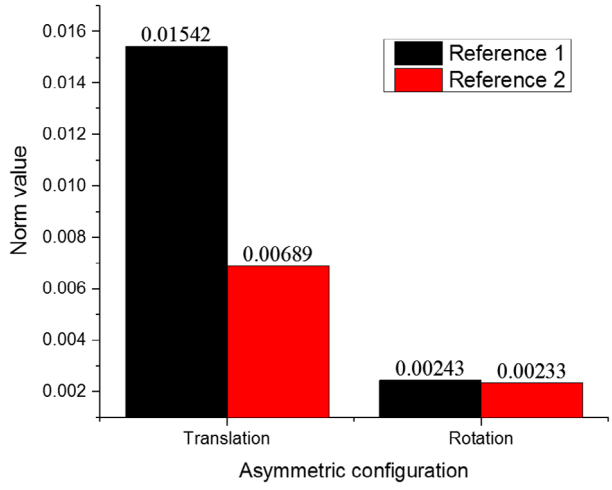

Figure 12. Deformation comparison of Refs. 1 and 2 in the asymmetric configuration.

models are built in this research for a stiffness comparison, since FEA methods can provide accurate stiffness analysis and many researchers have adopted the FEA methods to validate their results.

In the FEA analysis, the actuators are modeled using spring elements. Beam elements are used to model the mobile platform and the limbs of the PTPM. All the passive joints are assumed to be non-deformable. The cross sections of all the analyzed components are of the same solid circular shape, and the materials are the same. The geometrical and material properties are listed in Table 2. Since the stiffness of a parallel manipulator is a local property and dependent on its configuration. It is time-consuming to analyze the stiffness of all the configurations using the FEA method. As the configurations of Refs. 1 and 2 can be categorized into two groups based on whether they are rotational symmetric, this paper selects a rotational symmetric configuration, in which the actuators have the same displacement, and an asymmetric configuration, in which the actuators have different displacements. Table 4 lists the displacements of the actuators in the configurations. The same wrench $\mathbf{W} = \begin{bmatrix} 0 & 0 & 100 & 0 & 0 & 100 \end{bmatrix}$ is applied on the mobile platforms of Refs. 1 and 2. The unit vector of the wrench is $\begin{bmatrix} 0 & 0 & \sqrt{2}/2 & 0 & 0 & \sqrt{2}/2 \end{bmatrix}$, which has been used in the optimization.

Figures 11 and 12 show the deformation values of Refs. 1 and 2 in the symmetric and asymmetric configurations. The deformation value includes the norm of translations and the norm of rotations. From Figure 11, it can be seen that the norm of rotations of the mobile platform of Ref. 2 is much smaller than that of Ref. 1 under the same wrench in the symmetric configuration, although the difference between translations of Refs. 1 and 2 is not obvious. Figure 12 depicts that the norm of translations of Ref. 2 is about half of that of Ref. 1 in the asymmetric configuration, and the norm of rotations of Ref. 2 is slightly smaller than that of Ref. 1. The comparison result shows that the stiffness of Ref. 2 is higher than that of Ref. 1 in the symmetric and asymmetric configurations. This result is consistent with that shown in Figure 9.

7. Conclusion

This paper provides an optimization method for general triglide-structure parallel manipulators. The optimization aims to improve their dexterity, stiffness, and space utilization. The deformation of the mobile platform, the limbs, and the actuators is considered to obtain the stiffness

Downloaded by [Tel Aviv University] at 02:41 05 November 2017

matrix, while the deformation of the mobile platform has frequently been ignored by many other researchers. A novel stiffness index is used to measure the stiffness property related to applied external wrench. The variable physical size due to different postures of a general triglide is computed to obtain its ratio of space utilization without using an approximate regular shape to estimate its physical size. This method can be used to optimize all general triglides, and it can also be used to optimize specific triglides, such as the linear delta and orthoglide.

Comparing with published work, the proposed method is proven to be capable of providing optimal designs in terms of dexterity, stiffness, and space utilization. The stiffness comparison using a FEA method also shows that the solution obtained using the proposed method has higher stiffness in the symmetric and asymmetric configurations. Additionally, the inclusion of the stroke of the actuators into the design variables is capable of improving the performance of a general triglide further. Hence, the proposed method is competent for the optimization of general triglides and it is highly suggested to consider the stroke of the actuators in the optimization of a parallel manipulator.

Nomenclature

NSGA	Non-dominance sorting genetic algorithm
GDI	Global dexterity index
GSI	Global stiffness index
RWV	Ratio of workspace volume to its physical size
A	Inverse compliant Jacobian matrix
C	Compliance matrix
{{C}}_{t}	Constraints
F	Objective functions
f	Reaction forces
J	Kinematic Jacobian matrix
$\mathbf{J}_q$	Forward kinematic Jacobian matrix
$\mathbf{J}_x$	Inverse kinematic Jacobian matrix
K	Stiffness matrix
U	Strain energy
A	Area of a cross section
E	Elastic modulus
G	Shear modulus
I	Area moment of inertia
J	Polar moment of inertia
W	External wrench
$\mathbf{W}_u$	Unit wrench
X	Design variables
Φ	Entire workspace
$\delta\boldsymbol{\xi}$	Infinitesimal twist
k	Condition number of Jacobian matrix
κ_V	Stiffness index
η	Global dexterity index
η_κ	Global stiffness index
η_V	Ratio of workspace volume to physical size
V	Workspace volume
V_1	Constant physical size
V_2	Variable physical size
V_3	Overlapped physical size
R_a	Radius of the base plate
R_b	Radius of the mobile platform
l	Limb length
s_d	Full stroke of actuators
α	Angle between the actuator axis and the base plate
$\alpha_{\mathbf{lim}}, \beta_{\mathbf{lim}}$	Limits of rotation angles of passive joints
$\dot{x}$	Velocity of the mobile platform
$\dot{q}_i$	Velocity of the ith actuator
t_i	Unit vector of B_iC_i
s_i	Unit vector ofA_iC_i
A_b	Cross section area of spherical solid beams
E	Elastic modulus of the solid beams
G	Shear modulus of the solid beams
N	Transmission ratio of the gear box used in actuators
P	Lead of the lead screw used in actuators
$k_{\mathbf{tor}}$	Equivalent stiffness of the motor

Disclosure statement

No potential conflict of interest was reported by the authors.

Notes on contributors

Shijun Yan received his BEng degree from Xi'an Jiaotong University China in Mechanical Engineering and Automation in 2008, and master's degree from Beihang University China in 2011 in Aerospace Manufacturing Engineering. He pursued and received his PhD degree at the National University of Singapore in the area of hybrid robot for machining on complicated surfaces. He worked as a research fellow at the Mechanical Engineering Department at National University of Singapore from 2015 to 2016. His current research interests include robotic welding, welding pass planning, optimization design of parallel manipulators, and machining using hybrid robots.

Soh Khim Ong is an associate professor in the Mechanical Engineering Department at the National University of Singapore, and a Faculty Member of the NUS Graduate School for Integrative Sciences and Engineering. Her research interests are virtual and augmented reality applications in manufacturing, assistive technology and rehabilitation engineering,

Downloaded by [Tel Aviv University] at 02:41 05 November 2017

and development of innovative teaching and education applications. She has a Google Scholar citation of over 3919 and H-Index 36, published 5 books and over 300 international refereed journal and conference papers. She has received many accolades and is well known both internationally and nationally. SK Ong received the 2004 Outstanding Young Manufacturing Engineer Award from the US Society of Manufacturing Engineers, where she is the 1st ASEAN female to have received this award since the award was established. In August 2012, she is elected a Fellow of CIRP, The International Academy for Production Engineering, where she is the first from the Asia region and the fourth female fellow in the world to be elected. She has also received various other awards including the 2009 Emerging Leaders Award in Academia by the US Society for Women Engineers.

Andrew Y C Nee is a Professor of Manufacturing Engineering, Department of Mechanical Engineering, National University of Singapore (NUS) since 1989. He received his PhD and DEng from Manchester and UMIST, respectively. His research interest is in CAD of tools, dies, fixture design, virtual, and augmented reality applications in manufacturing, remanufacturing, and parallel robotics. He is a Fellow of the International Academy for Production Engineering (CIRP) and served as its president in 2012, a Fellow of the Society of Manufacturing Engineers (USA), and its Gold Medal recipient in 2014. He is the editor-in-chief of the International Journal of Advanced Manufacturing Technology (Springer). He has published over 500 refereed journal and conference papers, and 18 edited and authored books. Research awards include the Outstanding Young Manufacturing Engineer Award by the Society of Manufacturing Engineers (1982), IJPR Norman Dudley Award (2003), the IMechE Joseph Whitworth Prize (2010), IEEE Kayamori Award (1999). He has graduated 45 PhD students and has a Google Scholar citation of over 9500 and H-Index 52.

Downloaded by [Tel Aviv University] at 02:41 05 November 2017

References

[1] Merlet JP. Parallel robots – open problems. In: Proceedings of the 9th International Symposium of Robotics Research; 1999 Oct 9–12; Snowbird, USA. p. 27–32.

[2] Khoukhi A, Baron L, Balazinski M. Constrained multi-objective trajectory planning of parallel kinematic machines. Rob. Comput-Integr. Manuf. 2009;25:756–769.

[3] Stock M, Miller K. Optimal kinematic design of spatial parallel manipulators: application to linear delta robot. J. Mech. Des. 2003;125:292–301.

[4] Yoshikawa T. Manipulability of robotic mechanisms. Int. J. Rob. Res. 1985;4:3–9.

[5] Tsai KY, Lin JC, Lo Y. Six-DOF parallel manipulators with maximal singularity-free joint space or workspace. Robotica. 2013;32:401–411.

[6] Pond G, Carretero JA. Formulating Jacobian matrices for the dexterity analysis of parallel manipulators. Mech. Mach. Theor. 2006;41:1505–1519.

[7] Liu H, Huang T, Chetwynd DG. A method to formulate a dimensionally homogeneous Jacobian of parallel manipulators. IEEE Trans. Rob. 2011;27:150–156.

[8] Hosseini MA, Daniali H-RM, Taghirad HD. Dexterous workspace optimization of a tricept parallel manipulator. Adv. Rob. 2011;25:1697–1712.

[9] Toz M, Kucuk S. Dexterous workspace optimization of an asymmetric six-degree of freedom Stewart–Gough platform type manipulator. Rob. Auton. Syst. 2013;61:1516–1528.

[10] Gosselin C, Angeles J. A global performance index for the kinematic optimization of robotic manipulators. J. Mech. Des. 1991;113:220–226.

[11] Altuzarra O, Pinto C, Sandru B, et al. Optimal dimensioning for parallel manipulators: workspace, dexterity, and energy. J. Mech. Des. 2011;133:041007.

[12] Liu X-J. Optimal kinematic design of a three translational DoFs parallel manipulator. Robotica. 2006;24:239–250.

[13] Abbasnejad G, Daniali HM, Fathi A. Architecture optimization of 4PUS+1PS parallel manipulator. Robotica. 2011;29:683–690.

[14] Lou YJ, Liu GF, Li ZX. Randomized optimal design of parallel manipulators. Autom. Sci. Eng. IEEE Trans. 2008;5:223–233.

[15] Rao ABK, Rao PVM, Saha SK. Dimensional design of hexaslides for optimal workspace and dexterity. IEEE Trans. Rob. 2005;21:444–449.

[16] Wu G, Caro S, Bai S, et al. Dynamic modeling and design optimization of a 3-DOF spherical parallel manipulator. Rob. Auton. Syst. 2014;62:1377–1386.

[17] Kelaiaia R, Company O, Zaatri A. Multiobjective optimization of a linear Delta parallel robot. Mech. Mach. Theory. 2012;50:159–178.

[18] Chi Z, Zhang D. Stiffness optimization of a novel reconfigurable parallel kinematic manipulator. Robotica. 2011;30:433–447.

[19] Gao Z, Zhang D, Hu X, et al. Design, analysis, and stiffness optimization of a three degree of freedom parallel manipulator. Robotica. 2010;28:349–357.

[20] El-Khasawneh BS, Ferreira PM. Computation of stiffness and stiffness bounds for parallel link manipulators. Int. J. Mach. Tools Manuf. 1999;39:321–342.

[21] Klimchik A, Pashkevich A, Caro S, et al. Stiffness modeling of robotic-manipulators under auxiliary loadings. In: The ASME 2012 International Design Engineering Technical Conferences (IDETC) and Computers and Information in Engineering Conference (CIE); 2012 Aug 12–15; Chicago (IL).

[22] Klimchik A, Chablat D, Pashkevich A. Stiffness modeling for perfect and non-perfect parallel manipulators under internal and external loadings. Mech. Mach. Theory. 2014;79:1–28.

[23] Kucuk S. Energy minimization for 3-RRR fully planar parallel manipulator using particle swarm optimization. Mech. Mach. Theory. 2013;62:129–149.

[24] Cheng G, Xu P, Yang D, et al. Stiffness analysis of a 3CPS parallel manipulator for mirror active adjusting platform in segmented telescope. Rob. Comput-Integr. Manuf. 2013;29:302–311.

[25] Wang Z-F, Ji S-M, Wan Y-H, et al. Optimal design of parallel robots for the prescribed regular dexterous workspace. In: *Mech. Mach. Theory*; 2007 Aug 18–21; Jinan, China. p. 563–568.

[26] Budde C, Last P, Hesselbach J. Development of a triglide-robot with enlarged workspace. In: Robotics and Automation, 2007 IEEE International Conference; 2007 Apr 10–14; Roma, Italy. p. 543–548.
[27] Chablat D, Wenger P. Architecture optimization of a 3-DOF translational parallel mechanism for machining applications, the orthoglide. IEEE Trans. Rob. Autom. 2007;2000:1–8.
[28] Fonseca CM, Fleming PJ. An overview of evolutionary algorithms in multiobjective optimization. Evol. Comput. 1995;3:1–16.
[29] Deb K, Pratap A, Agarwal S, et al. A fast and elitist multiobjective genetic algorithm: NSGA-II. IEEE Trans. Evol. Comput. 2002;6:182–197.
[30] Clavel R. Device for the movement and positioning of an element in space. US patent 4976582. 1990.
[31] Hebsacker M, Treib T, Zirn O, et al. Hexaglide 6 DOF and triaglide 3 DOF parallel manipulators. In: Mas CRB, Molinari-Tosatti L, Smith KS, editors. Parallel kinematic machines. 1st ed. London: Springer; 1999. p. 345–355.
[32] Wenger P, Chablat D. Kinematic analysis of a new parallel machine tool: the orthoglide. In: Lenarčič J, Stanišić MM, editors. Advances in robot kinematics. Springer; 2000. p. 305–314.
[33] Yan SJ, Ong SK, Nee AYC. Stiffness analysis of parallelogram-type parallel manipulators using a strain energy method. Rob. Comput.-Integr. Manuf. 2016;37:13–22.
[34] Merlet J. Parallel robots. 2nd ed. Dordrecht: Springer-Verlag; 2006. p. 266–274.
[35] Xu Q, Li, Y. GA-based architecture optimization of a 3-PUU parallel manipulator for stiffness performance. In: Intelligent Control and Automation, 2006. WCICA 2006. The Sixth World Congress; 2006 Jun 21–23; Dalian, China. p. 9099–9103.
[36] Courteille E, Deblaise D, Maurine P. Design optimization of a Delta-like parallel robot through global stiffness performance evaluation. In: 2009 IEEE/RSJ International Conference on Intelligent Robots and Systems; 2009 Oct 10–15; St. Louis, USA. p. 5159–5166.
[37] Kim HS, Tsai L-W. Design optimization of a cartesian parallel manipulator. J. Mech. Des. 2003;125:43–51.
[38] Liu X-J, Jin Z-L, Gao F. Optimum design of 3-DOF spherical parallel manipulators with respect to the conditioning and stiffness indices. Mech. Mach. Theory. 2000;35:1257–1267.
[39] Li Y, Xu Q. A new approach to the architecture optimization of a general 3-PUU translational parallel manipulator. J. Intell. Rob. Syst. 2006;46:59–72.

Downloaded by [Tel Aviv University] at 02:41 05 November 2017